Vol. 4, 4, 295–323 (1997)

Archives of Computational Methods in Engineering
State of the art reviews

Computational Simulation of Internal Bone Remodeling

H.E. Pettermann, T.J. Reiter† and F.G. Rammerstorfer∗

Institute of Lightweight Structures and Aerospace Engineering
Vienna University of Technology, Austria
Gusshausstr. 27–29 / E317
A–1040 Vienna, Austria

Summary

A review of the state of the art in computational modeling and analysis of the mechanical behavior of living bone is given. Particular attention is placed on algorithms for the simulation of the stress or strain induced remodeling processes. A special remodeling algorithm is presented which allows the simulation of internal bone remodeling taking into account not only adaptation of the spatial distribution of the effective mass density, but also the adaptation of the orientation of the material axes and of the orientation dependent stiffness parameters. Such remodeling algorithms require a sound formulation of the constitutive relations of bony material. For this purpose some micro-macro mechanical descriptions of bone in its different microstructural configurations are discussed. In conjunction with the above mentioned remodeling algorithm a new unified material model is derived for describing the linear elastic, orthotropic behavior of bone in the full range of micro-structures of cancellous and cortical bone. The application of the novel remodeling algorithm is demonstrated in an example.

INTRODUCTION

It is widely accepted that bone material has the ability to respond to changes in its mechanical loading environment (i.e. changes in the stress and strain fields) by adapting its shape and/or its internal micro-structure. These two aspects are commonly referred to as surface and internal remodeling [Frost 1964]. Bone material is resorbed in regions exposed to small load levels, whereas in highly stressed zones deposition of new bone material sets in. This process of functional adaptation is thought to enable bone to perform its mechanical function with a minimum of mass. However, as clinical practice shows, it can often be detrimental to the long term success of prostheses and implants used in orthopedic or dental surgery.

Though significant research has been undertaken to identify possible physical and biochemical phenomena which transform mechanical stresses and strains into actual bone cell processes (for a comprehensive overview see e.g. [Martin, Burr 1989]) these mechanisms remain not fully understood. Considerable attention has been focused on the development of phenomenologically based numerical simulation tools for predicting the results of the natural adaptation processes [e.g. Carter *et al.* 1987; Carter *et al.*, 1989; Cowin, Hegedus 1976; Cowin 1987; Huiskes *et al.* 1987; Hart, Davy 1989; Reiter *et al.* 1990; Beaupré *et al.* 1990; Prendergast, Taylor 1992]. Most of these approaches assume bone material to show isotropic linear elastic behavior and reflect the remodeling processes by adaptation of the bone apparent density and, introducing appropriate stiffness–density relations, by adaptation of the Young's modulus. Up till now, only a limited number of attempts have been undertaken to expand these models to more complex material symmetries, which better reflect the anisotropic behavior of actual bony tissue [Bucháček 1990; Carter *et al.* 1989;

† present address: VAI, Linz, Austria
∗ corresponding author

©1997 by CIMNE, Barcelona (Spain). ISSN: 1134–3060 Received: August 1996

Cowin *et al.* 1992; Fyhrie, Carter 1986; Jacobs *et al.* 1995; Pettermann 1993; Reiter 1996; Starke *et al.* 1992; Zysset, Curnier 1995] A more comprehensive description of the state of the art in bone remodeling simulation can be found in section "Remodeling Algorithms" of this paper.

As long as physiologically relevant stress states within the range of balanced adaptation of bone are considered, the remodeling process of secondary bone can, in an approximative manner, be described by assuming linear elastic behavior of bone. In the following section an overview on the description of the elastic behavior of bone is presented. With respect to computational simulations of bone remodeling a material law is required which allows a consistent and continuous transition between different micro-structures of cancellous bone as well as between cancellous and cortical bone. This means that a smooth change of the apparent density, of the elastic parameters in the anisotropic material description, and of the angles of the material axes must be represented in a unified manner.

Such a unified material law is described in the section "Material Laws for Bone" of this paper and an algorithm for the simultaneous adaptation of the anisotropic (i.e. orthotropic) stiffness and the local material orientation for internal remodeling is shown in the section "Remodeling Algorithms".

MATERIAL LAWS FOR BONE

Bone tissue generally can be classified as either highly densified cortical (or compact) bone, found at the surfaces of most bones and particularly in the shafts of long bones, or cancellous (or trabecular) bone, which shows a considerably smaller apparent density and is found only in the interior of bones. Both types show the same principal molecular-scale micro-structure, consisting of a hydroxyapatite reinforced collagenous matrix organized in a lamellar compound. The structural organization at the mesoscopic level, however, is totally different.

The overall material behavior of cancellous bone has been shown to be highly dependent on the trabecular volume fraction (which is directly related to the bone apparent density), on the stiffness of the bulk trabecular material, and on the three dimensional arrangement of the trabecular rods and plates, leading, in general, to anisotropic overall behavior. The majority of experimental investigations were focused on the uniaxial stiffness of cancellous bone specimens (mostly taken from the proximal femur or tibia) utilizing mechanical compression, tension and bending techniques as well as ultrasound methods. They showed strong evidence for a power-law relationship between apparent density and uniaxial Young's modulus of cancellous bone with reported exponents in the range of one to three. More recently a number of experimental studies were published concerning the actual anisotropic trabecular overall material behavior [e.g. Townsend *et al.* 1975; Goldstein *et al.* 1983; Rice *et al.* 1988; Hayes, Snyder 1989; Turner *et al.* 1990; Hollister *et al.* 1991; Goulet *et al.* 1994; van Rietbergen *et al.* 1995]. In addition to experimental investigations, a number of theoretical studies were performed based on micro-mechanical models for the simulation of the stiffness behavior of cancellous bone. McElhaney *et al.* [1970] reported a *porous block* model of cancellous bone, the stiffnesses being simulated by parallel or serial assemblages of springs. Pugh *et al.* [1973] proposed trabecular bone to be modeled by a collection of plates, concluding that bending and buckling were major modes of deformation of the trabeculae. Williams and Lewis [1982] used a plane strain (two dimensional) Finite Element model of an actual tissue section to compute its elastic behavior. Analytical models were developed, which describe trabecular bone as a connected network of rods and plates [Gibson 1985; Gibson, Ashby 1988]. Christensen [1986] focused on three dimensional isotropic high porosity open and closed cell materials, assuming axial deformation of the cell walls and finding a linear relationship between the stiffness parameters (Young's and shear moduli) and the bulk material volume fraction. Beaupré and Hayes [1985] introduced a three dimensional unit-cell model of open-cell trabecular structure consisting of a cube containing a spherical hole, the diameter of which was assumed to be larger than the cube's edge-length. In order to calculate the stiffness behavior of such a unit-cell under appropriate displacement boundary conditions, the Finite Element method was applied. A similar unit-cell approach was used by Hollister and co-workers using two dimensional [Hollister *et al.* 1990] unit-cells with circular voids and three dimensional [Hollister *et al.* 1991] unit-cells representing closed cell and open cell trabecular micro-structures. For the evaluation of the elastic material behavior Hollister and co workers applied the homogenization theory [Suquet 1990]. Real structure Finite Element simulation has been carried out by Hollister *et al.* [1994], van Rietbergen *et al.* [1995] and Müller [1994].

Several attempts have been undertaken to simulate the elastic behavior of cortical bone, which has to be considered as a highly complex, hierarchically structured composite, by micro-mechanical methods originally developed for describing artificial composites. For a long time mainly two–phase micro-mechanical models based on the rules of mixture, e.g. Voigt- and Reuss- type models [Currey 1964; Katz 1971, Piekarski 1973; Lees, Davidson 1977; Katz, Meunier 1990], as well as the Hashin-Shtrikman bounds [Katz 1971; Piekarski 1973], were applied, which both are capable of giving bounds on the stiffness parameters of compact bone tissue. More recently, "multi-scale" micro-mechanical models were introduced (consisting of two or three hierarchical levels of homogenization), which better reflect the micro-structure of cortical bone. Katz [1981] used a two-level hierarchical fiber-reinforced composite model. More recently a similar model was introduced which uses a two dimensional generalized plane strain Finite Element unit-cell approach [Hogan 1989]. Limited collections of published empirical data which were obtained by standard mechanical testing of cortical bone specimens (mainly from femoral or tibial bones) or, alternatively, *via* ultrasonic techniques can be found in [Lipson, Katz 1984; Rice *et al.* 1988; Reilly *et al.* 1974; Van Buskirk, Ashman 1981].

In the following subsections a unified material law for describing the elastic behavior of bone is derived which is then used in the computational simulation of bone remodeling as described in section "Remodeling Algorithms".

A Material Law for Spongy Bone

Following Gibson [1985], Gibson and Ashby [1988] one can find at least three typical micro-structures in cancellous bone, representing the local degree of triaxiality of the stress state: *isotropic open cell structure* in the case of pronounced triaxiality of the stress state, *plated structure* in the case of predominantly biaxial stress state, and *prismatic structure* (or honey-comb structure) for an almost uniaxial stress state (Figure 1). Certainly, these distinctions or classifications cannot be used in a strict way, and there exist smooth transitions, both between these micro-structures of bone material, and from low density cancellous bone to highly densified cortical bone.

Let us introduce the relative density of bone material

$$\rho_r = \frac{\rho_a}{\rho_T} \tag{1}$$

where ρ_a and ρ_T are the apparent and the bulk mass density, respectively. The three typical micro-structures and the corresponding micro-mechanical models as described by Gibson and Ashby [1988] are shown in Figure 1 and Figure 2, respectively. The effective material data (with respect to the material axes as defined in Figure 2) obtained for these models are summarized in the following chapters.

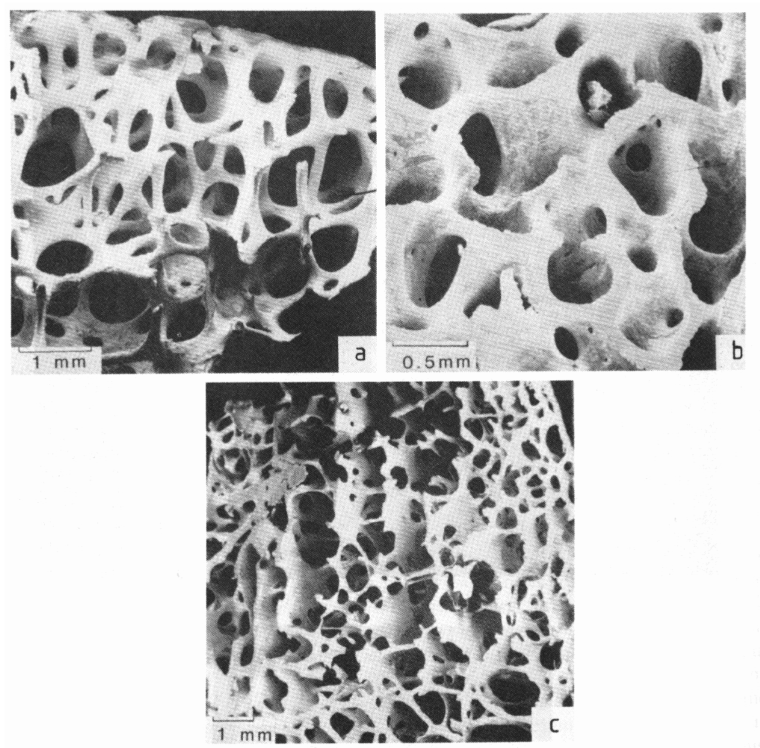

Figure 1. Different structures of cancellous bone. a) open cell structure, b) prismatic structure and c) plated structure [Gibson, Ashby 1988]

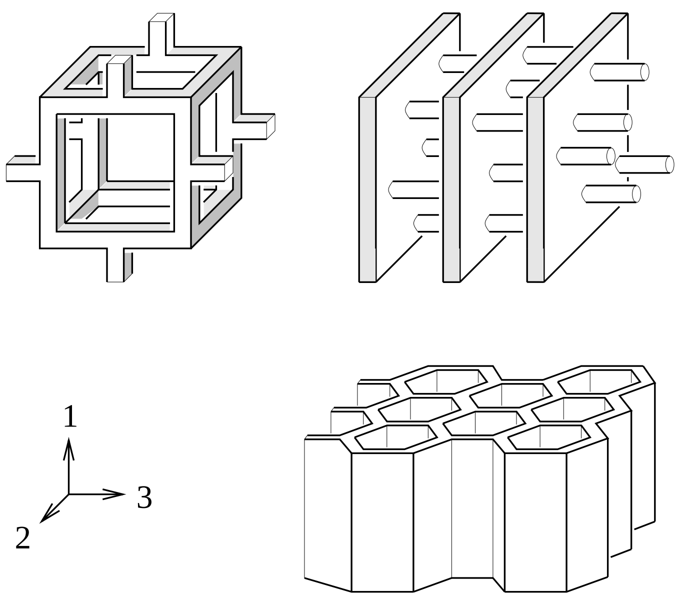

Figure 2. Micro-mechanical models for different structures of cancellous bone:open cell structure, plated structure and prismatic structure

Isotropic open cell structure

For the open cell structure, according to the model of Gibson and Ashby, the global stiffness is mainly governed by beam bending of the cell edges. Even though the unit cell of this model cannot be directly extended to three dimensions, an analogous smeared out, three dimensional behavior may be used. Thus, the structural Young's modulus is found to depend on the square of the relative density ρ_r and on the Young's modulus of the trabecular cell struts E_T as

$$E^* \approx E_T \, {\rho_r}^2 \tag{2}$$

From the structural model and from experimental observations on foams (but not on bone), and from the (assumed) isotropic global behavior, the Poisson ratio and the shear modulus follow as

$$\nu^* \approx \frac{1}{3} \tag{3}$$

$$G^* \approx \frac{E^*}{2(1+\nu^*)} \tag{4}$$

The tendency of more dense cancellous bone to form closed cells as reported e.g. in [Carter, Hayes 1977], can in principle be accounted for by closing the cell faces with membranes. However, it was observed [Müller 1994] that the densification of real bone material takes place by stiffening the struts rather than by building closing membranes. Thus, the open cell model can also be applied to describe the behavior of more dense isotropic bone.

Plated structure

Under the assumption that most of the material is concentrated in the plates the in-plane moduli of the plated structure are simply governed by the amount of trabecular material, expressed as a linear function of the relative density

$$E_1{}^* = E_2{}^* \approx E_T \, \rho_r \tag{5}$$

$$\nu_{12}{}^* = \nu_{21}{}^* \approx \nu_T \tag{6}$$

$$G_{12}{}^* \approx \frac{E_1{}^*}{2(1+\nu_{12}{}^*)} \tag{7}$$

For the out–of–plane direction, neglecting the compliance of the connecting rods, the stiffness is dominated by plate bending and therefore the Young's modulus is found to be proportional to the third power of the relative density

$$E_3{}^* \propto E_T \, {\rho_r}^3 \tag{8}$$

No other Poisson contraction will occur, so that

$$\nu_{13}{}^* = \nu_{23}{}^* = \nu_{31}{}^* = \nu_{32}{}^* \approx 0 \tag{9}$$

Only a rough estimate can be given for the out–of–plane shear moduli, expressed here in a form which is analogous to the other equations,

$$G_{13}{}^* = G_{23}{}^* \approx \frac{E_3{}^*}{2(1+\nu_{13}{}^*)} \tag{10}$$

Prismatic structure

The Young's modulus in the direction of the prisms' axis depends only on the amount of material, because no effects due to structural deformation of the honeycomb cells will occur

$$E_1{}^* \approx E_T\ \rho_r \tag{11}$$

The axial Poisson ratios are found to be approximately the same as for the trabecular material

$$\nu_{12}{}^* = \nu_{13}{}^* \approx \nu_T \tag{12}$$

and the transverse ones are nearly zero due to neglectable interaction

$$\nu_{21}{}^* = \nu_{31}{}^* \approx 0 \tag{13}$$

Using the theorems of minimum potential energy and of minimum complementary energy, Gibson and Ashby [1988] derived the shear moduli (for regular hexagons) as

$$G_{12}{}^* = G_{13}{}^* \approx \frac{1}{2}\ \frac{E_1{}^*}{2(1+\nu_{13}{}^*)} \tag{14}$$

The structural deformation of the regular hexagons gives rise to the Young's moduli in the isotropic plane, which show a cubic dependence on the relative density

$$E_2{}^* = E_3{}^* \approx 1.5\ E_T\ \rho_r{}^3 \tag{15}$$

The structural model predicts the in–plane Poisson ratios as

$$\nu_{23}{}^* = \nu_{32}{}^* \approx 1 \tag{16}$$

and the isotropic relation for the in–plane shear modulus holds

$$G_{23}{}^* \approx \frac{E_3{}^*}{2(1+\nu_{23}{}^*)} \tag{17}$$

For each of these three "basic" micro-structures the trabecular bone material making up the struts and plates is treated as isotropic (even though it is a highly anisotropic, lamellar composite structure). For the structural stiffness of the bone material, however, the above assumption appears to be a good approximation, because the bending of plates and struts is dominated by the in-plane stiffness and the stiffness in direction of the struts, respectively.

It should be noted that the materail models introduced in this section describe either isotropic or transverse isotropic elastic material behavior.

The Concept of Orthotropy Parameters

Now let us introduce "orthotropy parameters" β_i which are defined as follows

$$E_i^* \propto \rho_r^{\beta_i} \tag{18}$$

where the indices i describe the axes of the principal stresses, which are assumed to be aligned with the related material axes (an assumption which will be commented on later), ordered according to

$$|\sigma_1| \geq |\sigma_2| \geq |\sigma_3| \tag{19}$$

We find the following vectors of orthotropy parameters $\underset{\sim}{\beta}$ corresponding to the above "basic" micro-structures and related to the material axes as defined in Figure 2, $\underset{\sim}{\beta}^T = (2,2,2)$ for the isotropic structure, $\underset{\sim}{\beta}^T = (1,1,3)$ for the plated structure, $\underset{\sim}{\beta}^T = (1,3,3)$ for the prismatic structure, respectively. In general, the real micro–structure of cancellous bone cannot be described by the above "basic" configurations based on Gibson, Ashby [1988], but may be regarded as some intermediate structure. The degree of triaxiality of the local stress state, the cancellous structure is exposed to determines whether the appearance of bone is rather related to one of the "basic" micro–structures or somewhere in–between. In order to give a quantitative formulation to this rather qualitative statement we introduce the following assumption for the dependence of the orthotropy parameters on the stress state

$$\beta_i = 3 - |\sigma_i| \; \frac{2}{|\sigma_1| + |\sigma_3|} \tag{20}$$

with σ_i denoting the principal stress components. Together with eq.(19) this gives rise to the following relations for the orthotropy parameters

$$\beta_1 \leq \beta_2 \leq \beta_3 \tag{21}$$

$$\beta_1 \in [1.0, 2.0] \quad , \qquad \beta_2 \in [1.0, 3.0] \quad , \qquad \beta_3 \in [2.0, 3.0] \tag{22}$$

This heuristic assumption provides a continuous transition between the three "basic" micro-structures for intermediate stress states and is consistent in the following sense: Equation (20) exactly reproduces the vectors of orthotropy parameters for the three "basic" micro-structures, if the corresponding stress state is present. This can easily be checked by inserting the relevant stress states expressed in terms of principal stresses into eq.(20) (assuming that the material axes coincide with the principal stress axes).

$$|\sigma_1| = |\sigma_2| = |\sigma_3| \rightarrow \underset{\sim}{\beta}^T = (2,2,2) \quad \ldots \quad \text{isotropic structure}$$

$$|\sigma_1| = |\sigma_2| \neq 0 \wedge |\sigma_3| = 0 \rightarrow \underset{\sim}{\beta}^T = (1,1,3) \quad \ldots \quad \text{plated structure}$$

$$|\sigma_1| \neq 0 \wedge |\sigma_2| = |\sigma_3| = 0 \rightarrow \underset{\sim}{\beta}^T = (1,3,3) \quad \ldots \quad \text{prismatic structure}$$

Although the "basic" micro-structures show isotropic or transverse isotropic material behavior the concept of orthotropy parameters can give rise to general orthotropic descriptions of bone material as will be shown later.

The range of validity of the above models is given by Gibson and Ashby [1988] for a relative density of $\rho_r \leq 0.3$. To obtain the unified model these equations are also used in the range of more densified cancellous bone. Even though the deformation behavior becomes different at higher relative densities, reasonable values for the Young's moduli are obtained (at least in the sense of a continuous transition) (Figure 5). This way the elastic constants for the whole range of micro-structures in cancellous bone can be captured by a single set of equations as described later.

A Material Law for Cortical Bone

In order to define the transition between cancellous and cortical bone we introduce a transition value of the relative mass density $\rho_{r,t}$

$$\begin{aligned} \rho_r < \rho_{r,t} \quad &\rightarrow \quad \text{cancellous bone} \\ \rho_r > \rho_{r,t} \quad &\rightarrow \quad \text{cortical bone} \end{aligned}$$

Furthermore, we assume a maximum relative density for compact bone in the most densified configuration $\rho_{r,max}$ (≈0.95 for "healthy" secondary compact bone), as well as the Young's moduli and the Poisson ratios, respectively, in this configuration: $E_{C,max}, E_{C,min}$ and $\nu_{C,12}, \nu_{C,13}, \nu_{C,23}$ (under the assumption $E_{C,max} = E_{C,1} \geq E_{C,2} \geq E_{C,3} = E_{C,min}$, where $E_{C,i}$ are the Young's moduli of the most dense configuration in the principal material coordinate system). In the present unified model provision is made for introducing these Young's moduli independently from the trabecular Young's modulus, because experimental observations have shown a significantly higher value for the stiffest direction in compact bone than for trabecular bone [Rho *et al.* 1993]. These data allow an interpolation (assumed to be linear with respect to $\rho_r \in [\rho_{r,t}, \rho_{r,max}]$ for the sake of simplicity) between highly densified cancellous bone and highly densified compact bone, leading to a set of equations for the elastic constants of the cortical bone depending on its relative mass density and the degree of triaxiality of the stress state.

Formulation of a Unified Material Law for Bone

As mentioned above, internal remodeling simulations require a unified material description of bone in the whole range of apparent densities which is given by an expression of the following form

$$\underset{\sim}{\sigma} = \underset{\approx}{\mathbf{E}}\underset{\sim}{\varepsilon} \qquad \text{with} \qquad \underset{\approx}{\mathbf{E}} = \underset{\approx}{\mathcal{E}}(\rho_r, \underset{\sim}{\beta}) \tag{23}$$

with respect to the spatially varying material axes. $\underset{\sim}{\sigma}$ and $\underset{\sim}{\varepsilon}$ are the 6×1 representations of the stress and strain tensors, respectively, and $\underset{\approx}{\mathbf{E}}$ is the 6×6 representation of the elasticity tensor. Although discussed later, it should be mentioned at this point that the arguments in $\underset{\approx}{\mathcal{E}}$, i.e. ρ_r and $\underset{\sim}{\beta}$, as well as the orientation of the material axes are subject to remodeling.

With the above assumptions and the given values for the description of the bulk material of the trabeculae, i.e. E_T, ν_T, the limiting values of ρ_r, i.e. $\rho_{r,t}$ and $\rho_{r,max}$, as well as the material constants for the most densified compact bone $E_{C,max}$ $E_{C,min}$ and $\nu_{C,12}$, $\nu_{C,13}$, $\nu_{C,23}$, the elastic parameters for determining the elasticity matrix $\underset{\approx}{\mathbf{E}}$ can be found in a continuous and unified manner.

In the unified material model the structure of cancellous bone must generally be classified as plated–type or prismatic–type. The distinction between plated–type and prismatic–type micro-structures is governed by the orthotropy parameter β_2

$$\begin{aligned} \beta_2 < 2 \quad &\rightarrow \quad \text{plated–type structure} \\ \beta_2 > 2 \quad &\rightarrow \quad \text{prismatic–type structure} \end{aligned}$$

All cases of $\beta_2 = 2$ must be captured by both classifications and can be regarded as intermediate states (isotropic structure is one special case of these intermediate states). Furthermore, a distinction between cancellous and cortical bone has to be made.

In order to state a unified model suitable for remodeling the material moduli (E_i, ν_{ij}, G_{ij}) must be expressed as continuous functions of the leading parameters (β_i, ρ_r). Within the range of cancellous bone this is done by an "interpolation" between the "basic" micro–structures. For cortical bone a linear interpolation between the fictitious $\underset{\sim}{\beta}$–related values corresponding to the transition density $\rho_{r,t}$ and the $\underset{\sim}{\beta}$–related values of the most dense compact bone is performed.

For cancellous bone the three Young's moduli follow from eq.(18) as

$$E_i = E_T {\rho_r}^{\beta_i} \tag{24}$$

where the proportionality factors have been neglected for the in-plane moduli of the prismatic structure and the out–of–plane modulus of the plated structure. This inaccuracy is of minor influence with respect to the global behavior, because the moduli for the corresponding directions (which depend on the third power of the relative density) are very small compared to those for the other directions. The alteration of the density dependent Young's modulus function corresponding to the use of orthotropy parameters deviating from $\beta_i = 2$ agree well with data published by Müller [1994].

For cortical bone we introduce the density ratio

$$\hat{\rho} = \frac{\rho_r - \rho_{r,t}}{\rho_{r,max} - \rho_{r,t}} \tag{25}$$

and a ratio of the Young's moduli of the most dense compact bone

$$\kappa = \frac{E_{Cmin}}{E_{Cmax}} \tag{26}$$

Then linear interpolation gives the cortical Young's moduli as

$$E_i = E_T \ {\rho_{r,t}}^{\beta_i} + (E_{Cmax} \ \delta_i - E_T \ {\rho_{r,t}}^{\beta_i})\hat{\rho} \tag{27}$$

$$\text{with} \quad \delta_i = \frac{\kappa - 1}{2}\beta_i + \frac{3 - \kappa}{2} \tag{28}$$

A consistent interpolation of the different Poisson numbers giving rise to continuous transitions for any possible change of the actual structure (within the framework of the unified model) is more complicated. For cancellous bone some Poisson ratios have fixed values and the others have to be calculated by means of $\underset{\sim}{\beta}$–related "extreme" values. Regarding cortical bone one has, in addition, to involve the fictitious values for most dense cancellous bone. The detailed equations for the Poisson numbers ν_{12}, ν_{13} and ν_{23} are given in the appendix. The remaining Poisson numbers can be calculated from the symmetry condition of the elasticity matrix $\frac{\nu_{ij}}{E_i} = \frac{\nu_{ji}}{E_j}$.

For the shear moduli of cortical bone of prismatic–type structure, where no structural model is used, the application of the relations derived for cancellous bone shows good agreement with experimentally observed data from long bones. The results given by Van Buskirk and Ashman [1981] can be met by the prismatic structure model using a slightly increased β_1-value (which corresponds to a nearly uniaxial case). For plated–type cortical bone, if it exists at all, no experimental data are available. Hence, the shear moduli of both cancellous and cortical bone are described by a set of equations differentiating only whether the structure type is plated–type or prismatic–type.

Prismatic–Type Structure:

$$G_{12} = \frac{\delta}{2} \frac{E_1}{2(1+\nu_{12})} \quad \text{with} \quad \delta = (\beta_2 - 2)\beta_1 + 6 - 2\beta_2 \tag{29}$$

$$G_{13} = \frac{\beta_1}{2} \frac{E_1}{2(1+\nu_{13})} \quad , \quad G_{23} = \frac{E_3}{2(1+\nu_{23})} \tag{30}$$

Plated–Type Structure:

$$G_{12} = \frac{E_1}{2(1+\nu_{12})} \quad , \quad G_{13} = \frac{E_3}{2(1+\nu_{13})} \quad , \quad G_{23} = \frac{E_3}{2(1+\nu_{23})} \tag{31}$$

From these "engineering" moduli (E_i, G_{ij}, ν_{ij}; $i,j = 1,2,3$), selected by use of β_2 and ρ_r, the compliance matrix $\underset{\approx}{\mathbf{C}}$ and the elasticity matrix $\underset{\approx}{\mathbf{E}}$ can be found in the usual way (using the 6×6 representation of the elastic tensors and engineering strains)

$$\underset{\approx}{\mathbf{C}} = \begin{pmatrix} \frac{1}{E_1} & -\frac{\nu_{21}}{E_2} & -\frac{\nu_{31}}{E_3} & & & \\ -\frac{\nu_{12}}{E_1} & \frac{1}{E_2} & -\frac{\nu_{32}}{E_3} & & & \\ -\frac{\nu_{13}}{E_1} & -\frac{\nu_{23}}{E_2} & \frac{1}{E_3} & & & \\ & & & \frac{1}{G_{12}} & & \\ & & & & \frac{1}{G_{13}} & \\ & & & & & \frac{1}{G_{23}} \end{pmatrix} \tag{32}$$

with the condition for the physically required symmetry $\frac{\nu_{ij}}{E_i} = \frac{\nu_{ji}}{E_j}$ and

$$\underset{\approx}{\mathbf{E}} = \underset{\approx}{\mathbf{C}}^{-1} \tag{33}$$

Since this elasticity matrix is related to the position dependent orientation of the material axes typical stress analysis procedures, such as the Finite Element method, require a rotational transformation to obtain the material law with respect to a global coordinate system

$$\underset{\sim}{\bar{\sigma}} = \underset{\approx}{\bar{\mathbf{E}}}\underset{\sim}{\bar{\varepsilon}} \quad \text{with} \quad \underset{\approx}{\bar{\mathbf{E}}} = \underset{\approx}{\mathbf{T}}\underset{\approx}{\mathbf{E}}\underset{\approx}{\mathbf{T}}^T \tag{34}$$

where the rotational transformation matrix

$$\underset{\approx}{\mathbf{T}} = \underset{\approx}{\mathcal{T}}(\phi_1, \phi_2, \phi_3) \tag{35}$$

is a function of the orientation of the material axes defined by the components of the *Rodriguez* rotation vector [Büchter, Ramm 1992] with respect to the global coordinate system.

Experimentally evaluated values for the exponent β of the density (e.g. Carter and Hayes [1977], Gibson [1985], Rice *et al.* [1988], Ashman and Rho [1988]) are bounded by the extreme values, viz. 1 and 3, introduced by the present model. Most of the experimental studies investigating the Young's modulus as a power law function of the mass density do not focus on the pertinent micro–structure and on a possible anisotropy of the material.

REMODELING ALGORITHMS - A REVIEW OF THE STATE OF THE ART

Clinical investigations carried out during the last decades have revealed strong evidence of the existence of functional adaptation and stress or strain induced remodeling processes acting in bone. Such bone remodeling reactions have been shown to be sensitive to the local strain rates, strain peak magnitudes, strain distributions, the principal dynamical nature of the loads, and to the number of loading cycles. Possible physical and biochemical phenomena transforming mechanical stresses and strains into actual bone cell processes were discovered and studied in some detail. All this experimental evidence has shown bone remodeling and functional adaptation to be of a rather complicated nature, which still cannot be readily described in detail.

Parallel to the efforts aimed at gaining insight into the nature of bone remodeling phenomena, a number of researchers worked on developing semiempirical, phenomenologically based mathematical descriptions of these processes, which are suitable for simulating and predicting actual stress related bone remodeling reactions. These mathematical formulations, which consider bone tissue to be a locally adaptive material, directly couple the mechanical loading, mostly characterized by the strain or stress tensors or measures calculated from them, with the local remodeling reactions as observed in experiments, *via* suitable "bone growth laws". Such growth laws are the basis of computational tools for simulating the natural adaptation occurring under given loading situations and changes in geometry and stiffness, as can be caused for example by implants. In the following an overview over several bone remodeling theories proposed by different authors is given.

The Model of Pauwels

One of the first mathematical formulations of "Wolffs law" was given by Pauwels [1965]. He assumed the existence of an optimal mechanical stimulus S_n, which has to be present in the bone tissue to ensure a balanced state of bone resorption and deposition. Pauwels was mainly interested in the surface remodeling of long bones which primarily are loaded by bending, so that the stress state can approximately be described as uniaxial. Hence, the remodeling relevant mechanical stimulus S was assumed to be identical with the axial stress σ. Consequently, the optimal value S_n corresponds to some optimal axial stress value σ_n. Stress values exceeding this optimal value will lead to an increase in osteoblastic activity giving rise to bone hypertrophy. Values below σ_n will lead to bone atrophy. This feedback system will force the stress state in the bone into the direction of the optimal homeostatic value as long as the actual stress lies within a certain range ($\sigma_u \leq \sigma \leq \sigma_o$ with $\sigma_n = \frac{\sigma_u+\sigma_o}{2}$). This principal idea can be formalized by a simple cubic relationship [Kummer 1972] as

$$\frac{dm}{dt} = c\ (\sigma - \sigma_u)\ (\sigma - \sigma_n)\ (\sigma - \sigma_o) \tag{36}$$

$\frac{dm}{dt}$ is the change in bone-mass per time, the coefficient c being a model parameter which has to be evaluated empirically. Numerical parameter studies of remodeling induced changes in a cross-section of a long bone (modeled as a hollow cylinder) subject to axial loading have shown that the value of c is rather critical with respect to the type of overall system behavior (damped oscillation, asymptotic convergence or undamped oscillation) [Kummer 1972].

The "Curvature" Model of Frost

Frost [1964] presented a somewhat different bone remodeling theory. The remodeling processes were thought to be controlled by a negative feedback system with some time-averaged strain acting as the control variable which has to surpass some threshold level to activate both osteoclastic and osteoblastic activity. In addition, the strain induced changes in the local curvature of the bone surface was assumed to have an inhibiting influence on either osteoclasts or osteoblasts. Strains resulting in more concave surfaces are assumed to lead to bone mass deposition whereas strains inducing less concave surfaces are subject to osteoclastic activity and, consequently, bone resorption. With this simple theory, it was possible to explain clinical results which show a tendency that fractured long bones that healed in a bent configuration straighten out during long term usage. Some years ago, the "curvature" model was reformulated in terms of strain gradients [Martin, Burr 1989].

The "Self–Optimazation" Concept of Carter *et al.*

In a series of papers Carter and co-workers introduced a mathematical formulation of the functional adaptation of trabecular bone based on a self-optimization concept [Carter *et al.* 1987; Whalen *et al.* 1988; Carter *et al.* 1989]. In accordance with Frost and Pauwels they assumed that a certain mechanical stimulus S has to be present in the bone tissue in order to maintain a quasi-stationary state of no bone remodeling. Carter *et al.* suggested this stimulus, which is thought to be constant in the whole bone, to be proportional to some effective stress measure

$$S \propto \sum_{i=1}^{l} n_i \bar{\sigma}^m_{eff\,i} \tag{37}$$

This formulation takes into account the influence of different load-cases $i (= 1 \ldots l)$ which are weighted by the corresponding number of load-cycles n_i and the influence of the magnitude of the corresponding stress states by introducing the exponent m. The effective stress measure $\bar{\sigma}_{eff\,i}(\underset{\sim}{\sigma}, \rho_a)$ is assumed to be a function of the local stress state $\underset{\sim}{\sigma}$ (corresponding to loadcase i), and of the local apparent density ρ_a. It is assumed that, whatever the biological basis of bone remodeling might be, functional adaptation gives bone the ability to maximize its structural integrity with the least amount of bone mass present. This is equivalent to the assumption that stress induced bone remodeling acts as an optimization tool minimizing some objective function (connected to some structural integrity criteria) [Fyhrie, Carter 1986]. Different possible optimization goals, including material strength and prevention of damage accumulation, have been addressed in the literature. In accordance with the assumed optimization goal a suitable selection of $\bar{\sigma}_{eff}$ has to be chosen. The utilization of a strain energy density approach is linked with the idea that bone is attempting to maximize its stiffness whereas a failure stress criterion is connected with material strength optimization. Both approaches can be formulated in a similar way leading to a correlation between the apparent density ρ_a and the effective stress measure $\bar{\sigma}_{eff}$ as

$$\rho_a \propto \left(\sum_{i=1}^{l} n_i \bar{\sigma}^m_{eff\,i} \right)^{\frac{1}{2m}} \tag{38}$$

Introducing the bulk strain energy density

$$U_b = \frac{\rho_c}{\rho_a} U \tag{39}$$

(U standing for the strain energy density in the "smeared out" or homogenized material and ρ_c being the maximum density of cortical bone), which better reflects the strain energy actually transmitted to the mineralized bone matrix, eq.(38) is rewritten as

$$\rho_a \propto \left(\sum_{i=1}^{l} n_i U_i^{\kappa} \right)^{\frac{1}{\kappa}} \tag{40}$$

where the exponent κ corresponds to the parameter m in eq.(38). Expression of this type give an estimate for the relation between the apparent density and an effective stress state in an optimal, i.e. equilibrium, state of no bone remodeling and can be used as "optimality criteria" in an iterative optimization procedure. In combination with the Finite Element method, which is employed for obtaining the stress and strain distributions in the proximal femur according to three different typical loading cases, these formulae were used to predict the apparent density distribution in the actual bone [Carter *et al.* 1987] starting from a homogeneous density distribution. The algorithms predicted density distributions similar to those found in the real femur within only a few iterations. However, no convergence could be obtained and further iterations led to non–physiological states where most elements showed either maximum or zero density values. Since the model addresses only the converged equilibrium state, time was not considered as a model parameter, and no specific estimates of the time history of the remodeling process were possible.

With respect to trabecular orientation Carter *et al.* followed the trajectorial hypothesis by assuming that the trabeculae are oriented in the direction of the principal stresses. It was shown that for a single load case an alignment between principal material and stress axes (and consequently strain axes) will result in an optimal configuration with respect to local stiffness maximization [Fyhrie, Carter 1986]. In the case of multiple load cases a weighted combination of the normal stress components with respect to a normal-vector $\vec{n}$ was suggested to serve as a stimulus for trabecular growth in the corresponding direction. This effective "cyclic normal stress" $\bar{\sigma_n}$ is calculated in analogy to eq.(40) as

$$\bar{\sigma}_n(\vec{n}) = \left[\sum_{i=1}^{l} \frac{n_i}{\sum_j n_j} \sigma_{n_i}^{\kappa}(\vec{n}) \right]^{\frac{1}{\kappa}} \tag{41}$$

The material stiffness in any direction $\vec{n}$ was suggested to be directly related to the magnitude of the corresponding cyclic normal stress $\bar{\sigma}_n$ [Carter *et al.* 1989]. However, no practical implementation of this trabecular orientation approach has been reported.

Starke *et al.* [1992] proposed the use of a modified version of the internal remodeling algorithm of Carter *et al.* in an investigation of the adaptive growth reactions of bone following total hip joint replacement. Bone material was assumed to show transversally isotropic material behavior, which reduces the number of independent material parameters compared to the orthotropic case. Following the trajectorial hypotheses of Wolff, the directions of the material axes are aligned with the principal stress directions. For example, the local longitudinal Young's modulus E_l is calculated in an iterative procedure as

$$E_l^{i+1} = c \left[\left(\sigma_{eff}^i (E_l^i) \right)^{2/(\kappa+1)} \right]^{\kappa} \tag{42}$$

where c and κ are suitable remodeling parameters. This procedure was implemented as a *User Material* subroutine in the nonlinear Finite Element program ABAQUS. Utilizing two- and three dimensional Finite Element models of a proximal femur and an implant-femur system the density distributions in the femoral bone before and after surgical treatment were predicted. Good agreement was found with actual density distributions known from natural femora in the case of the pre-surgery state. Pronounced stress shielding effects and, consequently, disuse resorption in the upper third of the cortical shaft were predicted for the implant-femur system.

The "Adaptive Elasticity" Model of Cowin *et al.*

Cowin and co–workers developed a sophisticated continuum theory of bone internal remodeling describing the deposition and resorption of bone material as the sum of chemical reactions between bone matrix and the extracellular fluids [Cowin, Hegedus 1976; Hegedus, Cowin 1976; Cowin, Nachlinger 1978].

This theory was used in the investigation of the evolution of bone inhomogeneity due to stress concentrations caused by elliptical holes [Firoozbakhsh, Aleyaasin 1989; Firoozbakhsh *et al.* 1992].

Taking into account the reorientation and the changes in the anisotropic material behavior of the trabecular architecture, Cowin *et al.* [1992] introduced a material model of trabecular bone utilizing the fabric tensor for expressing the anisotropy. The fabric tensor **H** is a symmetric second rank tensor, that gives a quantitative stereological description of the microstructural arrangement of trabeculae and pores [Turner *et al.* 1990] and can be related directly to the material elasticity tensor [Cowin 1985].

Cowin *et al.* [1992] suggested that the trabecular architecture attempts to adapt in such a way that some equilibrium strain state $\underset{\sim}{\varepsilon}^*$ is reached, which is characterized by

$$\underset{\sim}{\varepsilon}^* = (\varepsilon_1^0, \varepsilon_2^0, \varepsilon_3^0, 0, 0, 0)^T \tag{43}$$

where the $\varepsilon_i^0 (i = 1 \dots 3)$ are equal to some optimal values, which are different for tension and compression. Furthermore, it is assumed that for the equilibrium remodeling state the principal axes of the corresponding stress and strain states $\underset{\sim}{\sigma}^*$ and $\underset{\sim}{\varepsilon}^*$ must coincide with the principal axes of $\mathbf{H}^*$. In this state the bone material shows its equilibrium matrix volume fraction ξ^* and its equilibrium fabric tensor $\mathbf{H}^*$.

This model of orientational and anisotropic bone remodeling was used in a numerical simulation of trabecular remodeling reaction in a small (two dimensional) area subject to a change in the orientation of the applied stress field.

One of the major drawbacks of the model of Cowin lies in the relatively high number of bone remodeling parameters necessary for describing the remodeling behavior. Even in the linearized version each of the six components of the strain tensor is assumed to contribute to the remodeling process. Up to now quantitative estimates for these remodeling parameters have only been reported for a special class of problems in which it was possible to significantly reduce the number of parameters. In order to overcome this parameter identification problem Huiskes *et al.* [1987], following Carter *et al.*, suggested that the strain energy density (SED) may serve as a suitable mechanical stimulus in the case of surface and internal remodeling. In addition, an "equilibrium zone" of SED-values giving rise to no bone remodeling was proposed. Utilizing this modified version of the "Adaptive Elasticity" approach the density distribution in the proximal femur was predicted [Huiskes *et al.* 1987], resulting in a converged solution similar to the actual density patterns observed in real femora. In a further investigation the surface remodeling behavior of the femural cortical shaft around an intramedullary implant was studied (using a rather idealized two dimensional model with a straight stem). This study predicted pronounced resorption in the upper part of the cortical shaft due to a "stress shielding" effect of the stiff stem.

Reiter *et al.* [1990] extended the bone remodeling algorithm introduced by Huiskes *et al.* [1987] to include the effects of overstrain necrosis. A further refinement of the remodeling rules was given in Reiter *et al.* [1994] to account for certain biological bounds in the maximum bone material turnover. A detailed description of these extended bone remodeling algorithm can be found in [Reiter 1996]. These remodeling rules in combination with the Finite Element menthod were applied in a number of studies of the behavior of bone around implants in dental surgery [Reiter, Rammerstorfer 1993; Reiter *et al.* 1993a; Reiter *et al.* 1994a] and for simulating the behavior of the tibia after insertion of a knee endoprosthesis [Reiter *et al.* 1993b; Reiter *et al.* 1994a; Krach *et al.* 1995]. Pettermann [1993] proposed a further extension of the model used by Reiter *et al.* [1990] taking into account the anisotropic material behavior of bone tissue by introducing a unified bone material model. The application of these algorithms can be found in [Reiter *et al.* 1994b; Pettermann *et al.* 1995]. At this point it may be mentioned that modified versions of these algorithms have been adapted to topology and material optimization in technical applications, see for example [Reiter, Rammerstorfer 1993; Reiter *et al.* 1993b; Reiter 1995; Reiter 1996].

Recently the SED-based version of the adaptive elasticity approach was developed further by Harrigan and Hamilton [1992a; 1992b; 1993], who introduced a generalized continuum-level strain energy density U_T defined as

$$U_T = \frac{U}{\xi^m} \tag{44}$$

(ξ being the volume fraction of the mineralized matrix), as a mechanical stimulus for stress induced remodeling. In the case of the exponent m being equal to 1, U_T is proportional to the bulk-SED, defined in eq.(39). By introducing this slightly modified stimulus, the numerical remodeling simulation was shown to display a significantly more stable behavior. In [Reiter 1996] these phenomena are discussed in greater detail.

The original internal remodeling approach of Cowin *et al.* was extended to include material damping effects in bone tissue [Misra, Samanta 1987] by assuming the elasticity tensor to show time dependent behavior: $\underset{\approx}{\mathbf{E}} = \underset{\approx}{\mathbf{E}}^0\ f(t,e)$. The function $f(t,e)$ was selected to give a suitable relaxation function leading to a visco-elastic stress-strain relation.

Based on the idea that the changes in the density and orientation of bone material are not only influenced by the momentary strain regime but have to be considered to be functions of the whole strain history, Bucháček [1990] developed an extended version of the "Adaptive Elasticity" model of Cowin *et al.* He assumed that the difference between the actual density and material orientation and an optimal density and orientation, respectively, which both depend on the strain state, serve as the adaptive stimuli and have a time-fading effect on the remodeling behavior. This way, at a given time t any past strain event will have some effect on the remodeling changes but since some exponential time-fading function is assumed the bone reactions are dominated by the most recent strain events.

Cell Biology Based Remodeling Algorithms

Several researchers presented theoretical models in which some of the cell biology processes known to be involved in bone remodeling are explicitly taken into account. This way, mathematical formulations were obtained that are similar to the pure phenomenological descriptions given in the previous sections.

Beaupré *et al.* [1990] developed a time dependent description of bone internal remodeling where the remodeling reaction was proposed to depend on the difference between the actual bulk mechanical stimulus $S_{b,act}$, which is calculated according to eq.(37), and some site specific bulk equilibrium stimulus value $S_{b,eq}$, which is assumed to depend on the local apparent density. Furthermore, following the ideas of Martin [1984], the bone surface area available for osteoblastic and osteoclastic activity was taken into account.

Cell biology based model of Hart and Davy

Using mathematical formulations similar to those of the model of Cowin *et al.*, Hart and Davy [1989] established a cell biology based remodeling theory utilizing biological remodeling parameters that quantify processes of cell differentiation and cell function (numbers of different cells present and their average activity). According to Martin [1984], remodeling on the surfaces of bone (including intraosseos surfaces of canaliculae etc.) can be expressed as the sum of the osteoclast and osteoblast activity per unit area. Hart and Davy assumed the activity of the cells active in the remodeling process to be regulated by the cellular response to a strain dependent stimulus as

$$S(\vec{x},t) = \int_0^t f(\varepsilon_{ij}(\vec{x},t-\tau))\ d\tau \tag{45}$$

The activity levels of osteoblasts and osteoclasts (i.e. the average volume rate of bone that is deposed or resorbed by a single active osteoblast or osteoclast, respectively), $\dot{a}_b$ and $\dot{a}_c$ are given as

$$\dot{a}_b = c_b\ S\ + a_{b_0} \qquad , \qquad \dot{a}_c = c_c\ S + a_{c_0} \tag{46}$$

The scalar constants c_b, c_c, a_{b_0} and a_{c_0} are remodeling parameters to be evaluated empirically. Hart and Davy discussed various possible definitions of the strain dependent stimulus S utilizing higher order relationships as well as strain rate effects. In [Reiter 1996] it is shown that special forms of this sophisticated model can be related to some of the above described models.

Accumulated Damage Models

Bone remodeling has been considered to function as an effective self-healing procedure, which enables bone to avoid the accumulation of microdamage caused even by normal daily loading regimes. Prendergast and Taylor [1992] assumed that bone adaptation is directly regulated by the continuous process of tissue damage and repair. From the assumptions — 1) that there exists damage in the form of the distribution of microcracks at remodeling equilibrium and 2) that microcracks are repaired at a rate equal to that at which they are generated at remodeling equilibrium — they derived a mathematical formulation for local bone growth (or resorption).
This growth-law was introduced into an iterative procedure utilizing the Finite Element menthod for calculating the stress and, consequently, the damage distribution in the bone tissue around intramedullary fixated prostheses.

Viceconti and Seireg [1990] introduced a slightly different damage-based remodeling approach, utilizing an iterative procedure which accumulates the daily material damage and deposition. Viceconti and Seireg were able to qualitatively reproduce experimental data.

A NEW ALGORITHM FOR ANISOTROPIC INTERNAL REMODELING SIMULATION

In this section an improved remodeling algorithm is presented. It is based on the assumption that the adaptation of bony tissue with respect to site

specific mechanical stimuli, which act as the driving forces in the remodeling processes, can be described appropriately on the continuum level by using overall (smeared out) tissue material parameters and stress/strain measures. Any material parameter actually contributing to the local bone stiffness will be subject to a specific remodeling process which tries to adapt the effective stiffness behavior at the particular site under consideration according to the local stresses and strains. With respect to the unified material model presented above, which is based on micromechanical considerations, the essential material parameters governing the elastic material behavior of bony tissue are given by the apparent density ρ_a (or, alternatively, by the relative density, ρ_r), the structural anisotropy (orthotropy) described by the orthotropy parameters β_i and the orientation of the principal material axes with respect to some global coordinate system as described by the *Rodriguez* rotational vector $\underset{\sim}{\phi}$.

For each of these material parameters P (P standing for ρ_r, β_i or ϕ_i) a suitable remodeling stimulus S_P can be defined, which acts as a driving force in the remodeling process. Following Carter *et al.* [1987] and Huiskes *et al.* [1987], the difference between the effective (or actual) strain energy density (SED) $U_{T_{act}}$ and a homeostatic (or equilibrium) SED-value $U_{T_{eq}}$

$$S_\rho = U_{T_{act}} - U_{T_{eq}} \tag{47}$$

is assumed to be a suitable mechanical stimulus for the adaptation of apparent mass density (internal remodeling) as well as for external bone growth or resorption. In an analogous way the stimuli for changes regarding the degree of anisotropy as well as the orientation of the material axes can be defined, with the differences between the actual and the required equilibrium values again serving as the driving forces for adaptation, i.e.

$$S_{\beta_i} = \beta_{i,eq} - \beta_{i,act} \tag{48}$$

with $\beta_{i,eq}$ being defined according to eq.(20) and using the effective principal stress state as described below.

The orientational stimuli S_{ϕ_i} are chosen to be the difference between the components of the *Rodriguez* vectors describing the equilibrium material orientation and the actual material orientation

$$S_{\phi_i} = \phi_{i,eq} - \phi_{i,act} \tag{49}$$

The equilibrium material orientation is assumed to be identical with the directions of the principal stresses according to the local stress state. The hypothesis of bone tissue trying to develop into a state of coaligned principal material and stress directions, known as the *"trajectorial hypothesis"*, was introduced by Wolff [1892]. It is in good agreement with experimental findings [Hayes, Snyder 1989], and the alignment of the principal material and stress axes of orthotropic elastic low-shear materials has been shown to be optimal with respect to material stiffness [Fyhrie, Carter 1986; Pedersen 1989].

Following Carter *et al.* [1987] the effective strain energy density $U_{T_{act}}$ is calculated by an appropriate

superposition of a number (l) of relevant discrete load cases, weighted according to the corresponding number of load cycles.

$$U_{act} = \left(\sum_{i=1}^{l} \frac{n_i}{\sum_j n_j} U_{T_i}^k \right)^{\frac{1}{k}} \tag{50}$$

where k acts as a weighting parameter of the degree of influence of the load magnitude and the number of loading cycles n_i. U_T stands for a remodeling relevant SED-measure at the bone matrix-level. The transformation from the continuum level (smeared out) strain energy density U to the micro-structural bone matrix-level scale is represented according to eq.(44) as

$$U_T = \frac{U}{{\rho_r}^m} \tag{51}$$

where U is calculated from the local stress and strain state as

$$U = \frac{1}{2} \underset{\sim}{\sigma}^T \underset{\sim}{\varepsilon} \tag{52}$$

The exponent m was proposed to be equal to 1, so that it corresponds to an average bone matrix or "bulk"; SED [Carter *et al.* 1987; Huiskes *et al.* 1987; Reiter *et al.* 1990].

Large-scale Finite Element analyses of CT-scanned samples of actual trabecular bone areas showed the maximum actual matrix-level SED values to be orders of magnitude higher than the smeared out SED-value at the continuum level. Hollister *et al.* [1994] reported the maximum ratio of matrix to continuum level SED in their model to be as high as 350 and van Rietbergen *et al.* [1995] found a maximum ratio of 1029 with the mean ratio of $U_{T,max}/U$ being 7.07.

The effective stress state $\underset{\sim}{\sigma}_{act}$ for finding the orthotropy parameters (eq.(20)) and the orientation of the material axes, i.e. of the trabeculae, can be defined in analogy to eq.(50)

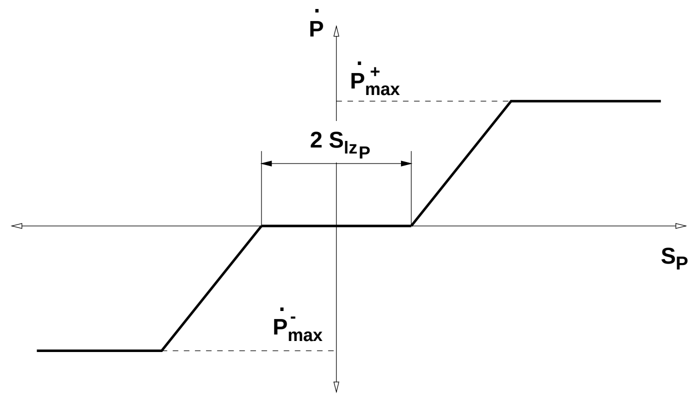

Figure 3. Qualitative graphical representation of the piecewise linear relationship between the remodeling stimulus S_P and the rate of remodeling changes $\dot{P}$

as an appropriate superposition of local stress tensors resulting from several distinct load cases

$$\underset{\sim}{\sigma}_{act} = \left(\sum_i \frac{n_i}{\sum_j n_j} \underset{\sim}{\sigma}_i{}^k \right)^{\frac{1}{k}} \tag{53}$$

Negative values of the stimulus $S_\rho < 0$ (cf. eq.(47)) lead to bone resorption whereas positive ones give rise to local bone hypertrophy, i.e. an increase in bone apparent density in the case of internal remodeling and growth of bone perpendicular to the bone surface in the case of surface remodeling, provided a limiting value above which overstrain necrosis appears is not exceeded (for details see [Reiter 1996]). For the other stimuli S_{β_i} and S_{ϕ_i} positive values lead to an increase, negative values to a decrease of the corresponding parameters β_i and ϕ_i, respectively. Each remodeling stimulus has to exceed a specific threshold level to cause any actual adaptive changes at all, which means that bone material is assumed to show a "lazy-zone" behavior in the vicinity of its homeostatic state. Furthermore, certain bounds on the growth rate (which are linked to biological cell activity limits) have to be taken into consideration.

The rate of adaptive change of the individual parameters can be described by a set of partial differential equations of the form

$$\frac{dP}{dt} = f\left(S_P(\vec{x}, t)\right) \tag{54}$$

A detailed investigation of these relations would require the consideration of the biochemical and bioelectrical processes controlling the activation of osteoblasts and osteoclasts which are not yet fully understood. For the sake of tractability and simplicity the connection between the individual stimuli and the resulting rates of change of the remodeling parameters are assumed to follow piecewise-linear relations (see Figure 3)

$$\frac{dP}{dt} = \begin{cases} C_{P1}\ (S_P + S_{lz_P}) & \text{for } S_P < -S_{lz_P} \\ 0 & \text{for } -S_{lz_P} \leq S_P \leq S_{lz_P} \\ C_{P2}\ (S_P - S_{lz_P}) & \text{for } S_{lz_P} < S_P \end{cases} \tag{55}$$

the rates of change being bounded by

$$\dot{P}^-_{max} \leq \frac{dP}{dt} = \dot{P} \leq \dot{P}^+_{max} \tag{56}$$

The parameter S_{lz_P} defining the range of the "lazy zone", and the constant coefficients C_{P1} and C_{P2} have to be established according to empirical data.

In order to follow the adaptational changes in time, the set of differential equations resulting from an element-wise application of eq.(54) with respect to a Finite Element discretization of the spatial domain has to be solved. At present a simple Euler forward time integration scheme is implemented, resulting in an iterative remodeling process as shown schematically in Figure 4. However, since the explicit Euler method is known to be only conditionally stable, the time steps are required to be sufficiently small to avoid numerical instabilities.

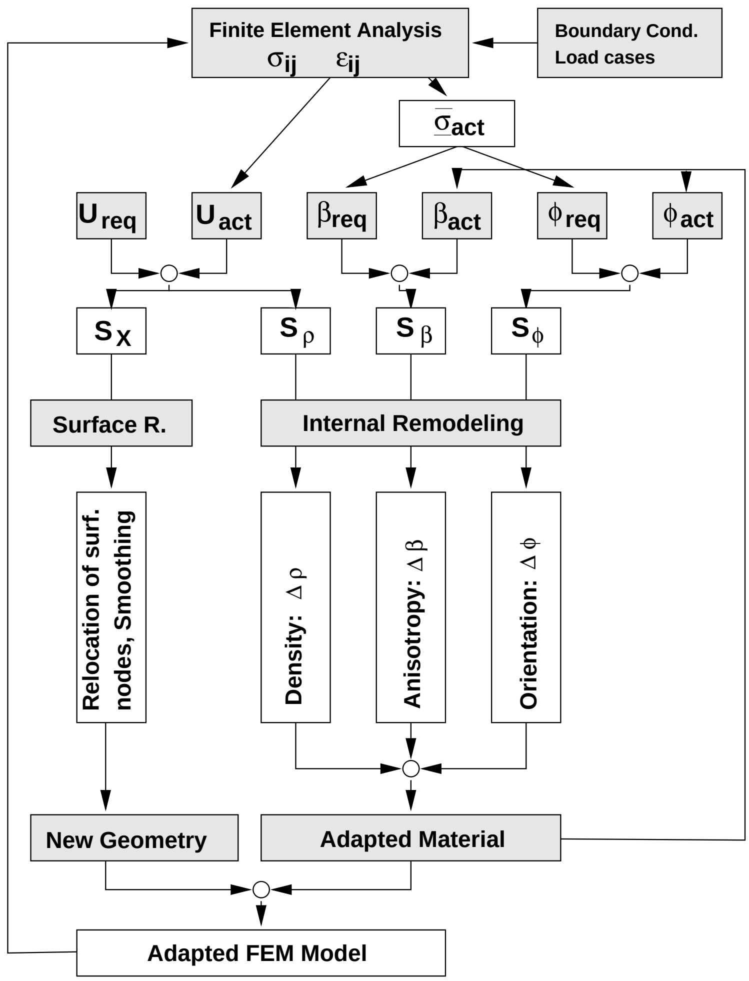

Figure 4. Schematic graphical representation of the iterative adaptive bone remodeling algorithm

Figure 5 gives a graphical illustration of a possible development of material anisotropy at a particular position starting from an isotropic material behavior, i.e. $\underset{\sim}{\beta}^T = (2.0,\ 2.0,\ 2.0)$, corresponding to a dominantly hydrostatic local stress state with $|\sigma_1| \approx |\sigma_2| \approx |\sigma_3|$ and $U_{act} = U_{eq}$). The local stress state is assumed to have changed (e.g. due to surgical treatment) so that it has become anisotropic ($|\sigma_1| > |\sigma_2| > |\sigma_3|$), giving rise to a higher effective SED ($U_{act} > U_{eq}$). According to the remodeling algorithm, the local material behavior will be subject to adaptive changes, which will tend to increase the material density and, consequently, will reduce the magnitude of the effective SED. In addition, the orthotropy parameters $\underset{\sim}{\beta}$ will develop in response to the new local stress state leading to an orthotropic material behavior. Immediately after the introduction of the change in the local stress state the rate of change will be rather high. However, the rate of change will subsequently decrease during the remodeling process while the system approaches a new remodeling equilibrium state.

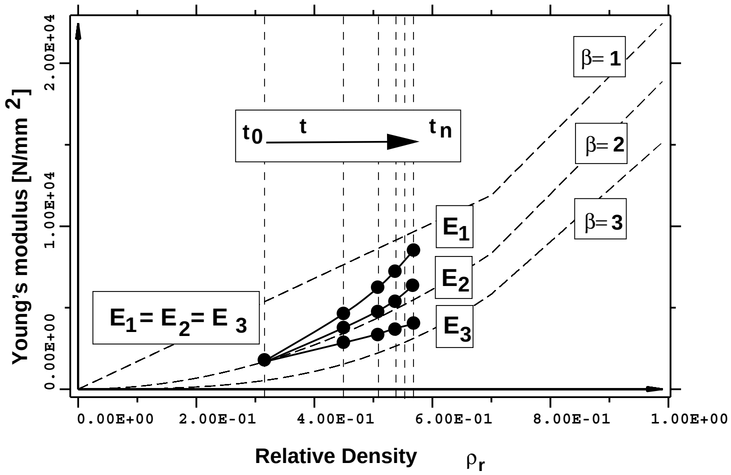

Figure 5. Qualitative graphical representation of the remodeling process due to changes in the local stress state. The development of anisotropic material behavior starting from an isotropic configuration is shown

The new remodeling algorithm can be used to predict the equilibrium configuration of a bone with respect to given loading conditions. If the progress of remodeling is of interest, emphasis has to be put on the formulation of the evolution in time, i.e. to a more precise determination of the remodeling parameters and the eventual interrelation between them. As a basic hypothesis for such interrelation, one may assume that the amount of resorbed and deposited bone material is kept to a minimum during each of the individual remodeling steps. In terms of the unified material model this means, that the orientation adaptation is done primarily for the smallest possible rotation which transforms the actual into the required orientation without regard of the indication of the axes.

Example: The Proximal Femur

Starting from an initial configuration of uniform apparent density ($\rho_a = 0.95$ g/cm^3) and isotropic material behavior, i.e. $\underset{\sim}{\beta}^T = (2.0,\ 2.0,\ 2.0)$, the density distribution, material orientation and anisotropy within the proximal femur predicted by the new internal remodeling algorithm are studied. For this purpose a highly idealized two dimensional model of the proximal femur with a plane stress state is assumed. This simplification is based on the observation that the external forces corresponding to appropriate representative load systems act mainly in the midfrontal plane of the femur. Accordingly, the relevant mechanical responses within the femur are dominated by inplane deformations and stresses. Following Carter *et al.* [1987] and Huiskes *et al.* [1987] it is assumed that the loading environment which the proximal femur is exposed to can be represented with sufficient accuracy by three typical load cases (see Figure 6 and Table 1).

Figure 7 shows a comparison between the distribution of the relative mass density as predicted by numerical simulation (left), and represented by an X-ray image of a typical femur (right). Bright areas indicate regions with low density trabecular bone, whereas dark zones represent high values of bone mass per unit area, i.e. high thickness and/or density of the bone. A smoothened image of the simulated density values, which are actually constant

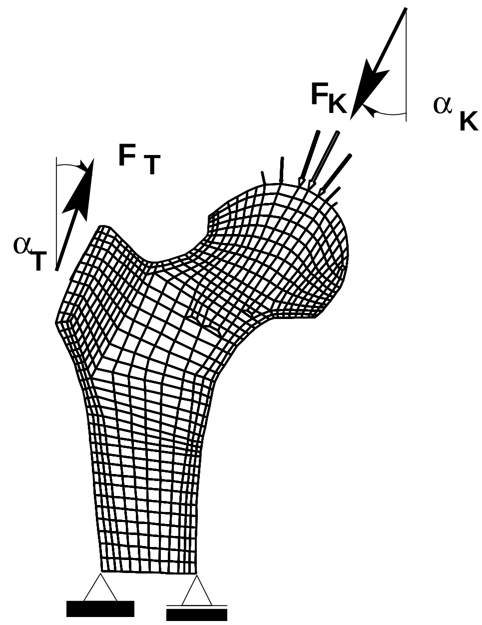

Figure 6. Two dimensional plane stress Finite Element model of a proximal femur, the loads are assumed to be cosine distributed. The magnitude and the direction of the load-resultants are given in Table 1

Load case	F_k [N]	α_k [°]	F_t [N]	α_t [°]
Load case 1	2317	24	702	28
Load case 2	1158	-15	351	-8
Load case 3	1548	56	468	35

Table 1. Magnitude and orientation of resultants of the loads applied to the model of the proximal femur; taken from [Huiskes *et al.* 1987]

in any element, is obtained by using a post-processing procedure which calculates averaged nodal values and employs a bilinear interpolation within the elements. The essential features, such as "Ward's triangle" and the high and low density regions within the femoral head are well represented in the numerical simulation results.

Figure 8 (right) gives the results of the numerical bone remodeling simulation with respect to the structural architecture, i.e. the pattern of orientation of the trabeculae within cancellous and of the Haversian systems within cortical bone, respectively, and, consequently, the anisotropic bone behavior. The orientations of the principal material directions (which are identical to the directions of the trabeculae and Haversian systems, respectively) within each element are represented by crosses pointing in the principal material directions with the lengths of the individual bars representing the effective stiffnesses of the bone in the corresponding directions. Again, the agreement between the numerical results and the structural architecture found in natural femora is reasonably good, compare Figure 8 (left). Some local disturbances in the density and material orientation patterns can be seen at the bottom of the Finite Element model, which are caused by the influence of the boundary conditions (see fig. 6). The results given in fig. 7 and 8 show the converged solution, which means that further iterations did not change the predicted distribution of the density and the elasticity tensors.

Figure 7. Density distribution in the proximal femur predicted by numerical bone remodeling simulation – smooth interpolation of density values (left); X-ray image [Kummer 1972] of a typical femur (right)

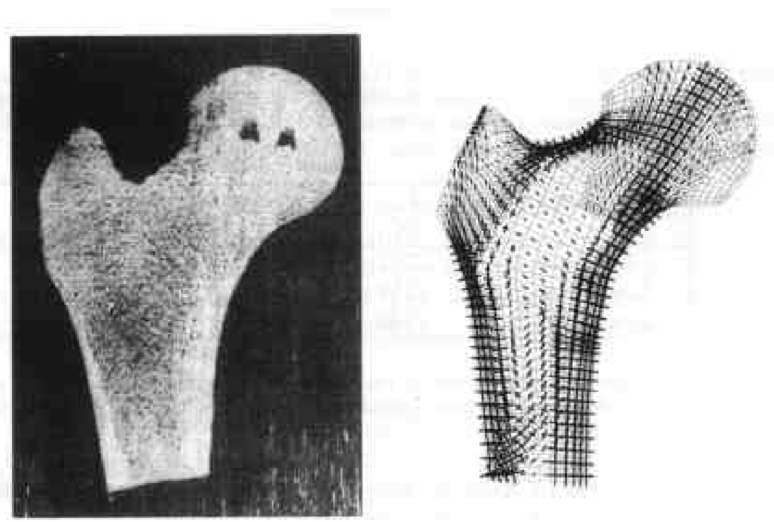

Figure 8. Cross section of a proximal human femur showing the trabecular architecture (left) [Gibson, Ashby 1988]; Predicted trabecular architecture within the proximal femur obtained by numerical simulation (right) with the direction of the crosses representing the material orientations and the lengths indicating the corresponding material stiffnesses within each element

Figure 9 displays the development of two convergence parameters (the values are normalized with respect to the first time step), viz. the relative average change in density $\overline{\Delta\rho_{rel}} = \overline{\Delta\rho_{a_i}}/\overline{\Delta\rho_{a0}}$ and the relative average difference between the actual and the equilibrium strain energy density $\overline{\Delta U_{act_{rel}}} = \overline{|S_{\rho_i}|}/\overline{|S_{\rho_0}|}$ with $S_{\rho_i} = U_{act_i} - U_{eq}$. A rather fast convergence of the solution can be observed within 20 to 30 time steps (this number is dependent on the actual values of the remodeling parameters used). After 50 time steps the solution can be considered to be fully converged. In order to account for the possibility of instabilities occurring in later time steps the simulation process was continued up to a total number of 500 increments with no further remodeling changes being found.

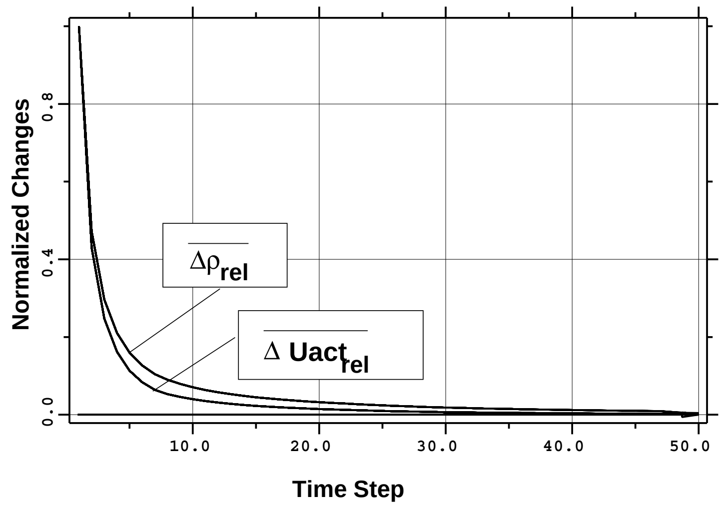

Figure 9. Graphical representation of the convergence behavior of the remodeling process during the simulation of the femoral architecture with respect to the relative average change in density $\overline{\Delta\rho_{rel}}$ and the relative average stimulus $\overline{\Delta U_{act_{rel}}}$. The parameters are normalized with respect to the starting configuration

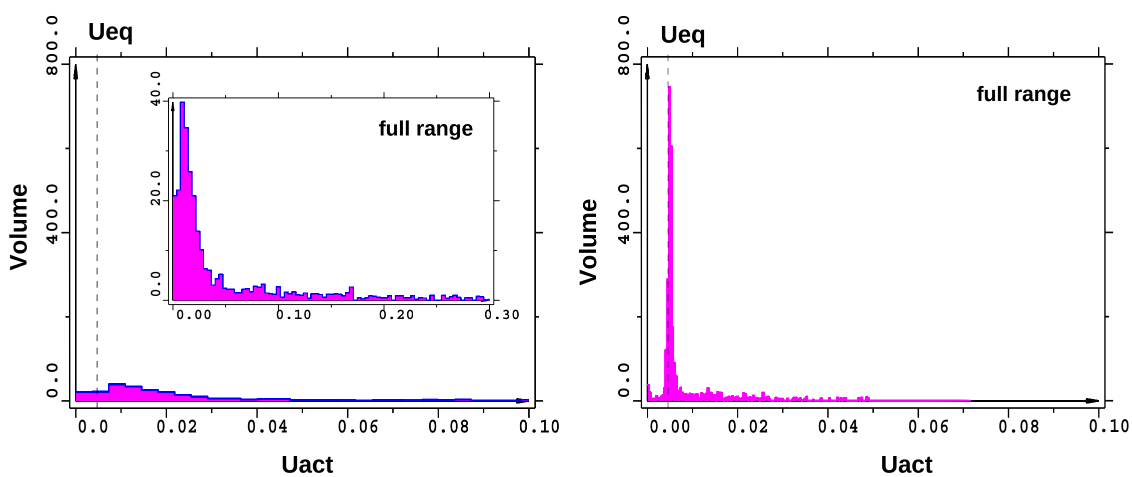

Figure 10. The distributions of effective strain energy density at the begin of the simulation (left) and for the converged solution (right)

Due to the remodeling process the system under consideration (i.e. the model of the femur subject to three different load cases) is driven towards an equilibrium state with a homogeneous distribution of the effective strain energy density with $U_{act} = U_{eq}$. Figure 10 gives a comparison of the distributions of U_{act} within the FE model of the femur for the starting configuration and for the converged state. Whereas at the start of the simulation the values of the effective SED are distributed over a wide range, in the converged solution the values of U_{act} show a narrow peak centered at the homeostatic SED value ($U_{eq} = 5.0\ 10^{-3}$ [Nmm^{-2} cm^3 g^{-1}]).

The plane model was chosen in the example because both the geometry of the proximal femur and the loading conditions relevant for remodeling as published in the literature, show a sufficient degree of symmetry with respect to the model plane. The algorithms described above are implemented for full 3/D simulation, corresponding test examples can be found in [Pettermann 1993; Reiter 1996].

CONCLUSIONS

Within physiological limits bone as a living tissue shows the ability of natural self-adaptation to altered stress fields. This adaptation or remodeling, respectively, appears in the form of surface, i.e. external, remodeling and/or microstructural, i.e. internal, remodeling. For both situations computational simulation algorithms exist for predicting the new balanced states after changes in the loading conditions (e.g. due to insertion of an implant). Such algorithms are discussed in the present review paper. All these algorithms require a proper description of biomechanically based laws for absorption or deposition of bone material. More advanced algorithms also include a proper simulation of the adaptation of the anisotropy. In each case a sound formulation of the material law of bone is necessary taking into account the location dependent micro-structural arrangements.

In the review a number of papers describing the mechanical behavior of bone material are discussed. Based on some of the results drawn from this literature a unified model for describing the linear elastic orthotropic behavior of bone has been derived and applied to internal bone remodeling. The material model is based on micro-mechanical models of cancellous bone with low density and experimentally evaluated material data for compacta at maximum density. It describes the elastic properties within the full range of architectures of bone, where the elastic moduli are given as continuous functions of the local density, structural appearance, and trabecular orientation. Experimentally evaluated (orthotropic) material data for bone of different densities (which are very rare) can be reproduced with good accuracy by applying the presented material model.

The remodeling algorithm described here in some detail allows the prediction of the balanced state of bone with respect to apparent mass density and micro-structure at least in a qualitative manner.

The presented unified materail model, which can be embedded in a number of remodeling algorithms reviewed in the paper, is considered as one possibility for studying internal remodeling while taking into account the anisotropy of bone material. It helps to improve the understanding of functional adaptation and may also be seen as a justification of the trajectorial hypothesis of Wolff.

ACKNOWLEDGMENTS

This work was partly supported by the *Österreichisches Bundesministerium für Wissenschaft, Forschung und Kunst* (Grant GZ 49.935/3–II/4/94) within the COST 512 action. Computer equipment was sponsored by the *Fonds "150 Jahre Technische Universität Wien" der Wiener Handelskammer* (Grant GZ 16402–02/001/93).

REFERENCES

1 Ashman, R.B., Rho J.Y. (1988), "Elastic Modulus of Trabecular Bone Material", *J. Biomech.*, **21**, pp. 177–181.

2 Beaupré, G.S. and Hayes W.C. (1985), "Finite Element Analysis of a Three–Dimensional Open–Cell Model for Trabecular Bone" *J. Biomed. Engng.*, **107**, pp. 249–256.

3 Beaupré, G.S., Orr T.E. and Carter D.R. (1990), "An Approach for Time–Dependent Bone Modeling and Remodeling — Theoretical Development", *J. Orthop. Res.*, **8**, pp. 651–661.

4 Bucháček, K. (1990), "Nonequilibrium Bone Remodelling: Changes of Mass Density and of the Axes of Anisotropy", *Int. J. Engng. Sci*, **28**, pp. 1039–1044.

5 Büchter, N. and Ramm, E. (1992), "Large Rotations in Structural Mechanics – Overview", In *Nonlinear Analysis of Shells by Finite Elements*, F.G. Rammerstorfer (Ed.), pp. 1–13, Springer-Verlag, Wien.

6 Carter, D.R. and Hayes, W.C. (1977), "The Compressive Behavior of Bone as a Two-Phase Porous Structure", *J. Bone Jt. Surg.*, **59-A**, pp. 954–962.

7 Carter, D.R., Fyhrie, D.P. and Whalen, R.T. (1987), "Trabecular Bone Density and Loading History: Regulation of Connective Tissue Morphology by Mechanical Energy", *J. Biomech.*, **20**, pp. 785–794.

8 Carter, D.R., Orr, T.E. and Fyhrie, D.P. (1989), "Relationship between Loading History and Femoral Cancellous Bone Architecture", *J. Biomech.*, **22**, pp. 231–244.

9 Christensen, R.M. (1986), "Mechanics of Low Density Materials", *J. Mech. Phys. Solids*, **34**, pp. 563–578.

10 Cowin, S.C. and Hegedus, D.H. (1976), "Bone Remodeling I: Theory of Adaptive Elasticity", *J. Elasticity*, **6**, pp. 313–326.

11 Cowin, S.C. and Nachlinger, R.R. (1978), "Bone Remodeling III: Uniqueness and Stability in Adaptive Elasticity Theory", *J. Elasticity*, **8**, pp. 285–295.

12 Cowin, S.C. (1985), "The Relationship between the Elasticity Tensor and the Fabric Tensor", *Mechanics of Materials*, **4**, pp. 137–147.

13 Cowin, S.C. (1987), "Bone Remodeling of Diaphysial Surfaces by Torsional Loads: Theoretical Predictions", *J. Biomech.*, **20**, pp. 1111–1120.

14 Cowin, S.C., Sadegh A.M. and Luo, G.M. (1992), "An Evolutionary Wolff's Law for Trabecular Architecture", *J. Biomech. Engng.*, **114**, pp. 129–136.

15 Currey, J.D. (1964), "Three Analogies to Explain the Mechanical Properties of Bone", *Biorheology*, **2**, pp. 1–10.

16 Firoozbakhsh, K. and Aleyaasin, M. (1989), "The Effect of Stress Concentration on Bone Remodeling: Theoretical Predictions", *J. Biomech. Engng.*, **111**, pp. 355–360.

17 Firoozbakhsh, K., Aleyaasin, M. and Moneim, M.S. (1992), "Evolution of Bone Inhomogeneity Around a Hole in an Orthotropic Plate of Bone: Theoretical Predictions", *J. Biomech.*, **25**, (4), pp. 387–394.

18 Frost, H.M. (1964), "*The Laws of Bone Structure*", Charles C. Thomas, Springfield, IL.

19 Fyhrie, D.P. and Carter, D.R. (1986), "A Unifying Principle Relating Stress to Trabecular Bone Morphology", *J. Orthop. Res.*, **4**, pp. 304–317.

20 Gibson, L.J. (1985), "The Mechanical Behavior of Cancellous Bone", *J. Biomech.*, **18**, pp. 317–328.

21 Gibson, L.J. and Ashby, M.F. (1988), "*Cellular Solids: Structure and Properties*", Pergamon Press, Oxford.

22 Goldstein, S.A., Wilson, D.L., Sonstegard, D.A. and Matthews, L.S. (1983), "The Mechanical Properties of Human Tibial Trabecular Bone as a Function of Metaphyseal Location", *J. Biomech.*, **16**, pp. 965–969.

23 Goulet, R.W., Goldstein, S.A., Ciarelli, M.J., Kuhn, J.L., Brown, M.B. and Feldkamp, L.A. (1994), "The Relationship Between the Structural and Orthogonal Compressive Properties of Trabecular Bone", *J. Biomech.*, **27**, pp. 375–389.

24 Harrigan, T.P. and Hamilton, J.J. (1992a), "An Analytical and Numerical Study of the Stability of Bone Remodeling Theories: Dependence on Microstructural Stimulus", *J. Biomech.*, **25**, pp. 477–488.

25 Harrigan, T.P. and Hamilton, J.J. (1992b), "Optimality Conditions for Finite Element Simulation of Adaptive Bone Remodeling", *Int. J. Solids Struct.*, **29**, pp. 2897–2906.

26 Harrigan, T.P. and Hamilton, J.J. (1993), "Finite Element Simulation of Adaptive Bone Remodelling: A Stability Criterion and a Time Stepping Method", *Int. J. Num. Meth. Eng.*, **36**, pp. 837–854.

27 Hart, R.T. and Davy, D.T. (1989), "Theories of Bone Modeling and Remodeling", In *Bone Mechanics*, S.C. Cowin (Ed.), CRC Press, Boca Raton, FL, pp. 253–277.

28 Hayes, W.C. and Snyder, B. (1989), "Toward a Quantitative Formulation of Wolff's Law of Trabecular Bone", In *Mechanical Properties of Bone*, S.C. Cowin (Ed.), AMD, **45**, ASME, New York, NY, pp. 43–68.

29 Hegedus, D.H. and Cowin, S.C. (1976), "Bone Remodeling II: Small Strain Adaptive Elasticity", *J. Elasticity*, **6**, pp. 337–352.

30 Hogan, H.A. (1989), "Micromechanics Modeling of Haversian Cortical Bone Properties", *J. Biomech.*, **22**, pp. 549–556.

31 Hollister, S.C., Kikuchi, N., Borodkin, J.L. and Goldstein, S.A. (1990), "A Study of Microstructural Analysis Methods: Implications for Modeling Trabecular Bone Microstructure", In *Advances in Bioengineering*, S.A. Goldstein (Ed.), BED, Vol. **17**, ASME, New York, NY, pp. 387–390.

32 Hollister, S.J., Fyhrie, D.P., Jepsen, K.J. and Goldstein, S.A. (1991), "Application of Homogenization Theory to the Study of Trabecular Bone Mechanics", *J. Biomech.*, **24**, pp. 825–839.

33 Hollister, S.J., Brennan, J.M. and Kikuchi, N. (1994), "A Homogenization Sampling Procedure for relating Trabecular Bone Effective Stiffness and Tissue Level Stress", *J. Biomech.*, **27**, pp. 433–444.

34 Huiskes, R., Weinans, H., Grootenboer, H.J., Dalstra, M., Fudala, B. and Sloof, T.J. (1987), "Adaptive Bone-Remodeling Theory Applied to Prosthetic-Design Analysis", *J. Biomech.*, **22**, pp. 1135–1150.

35 Jacobs, C.R., Simo, J.C., Beaupré, G.S. and Carter, D.R. (1995), "Comparing an Optimal Global Efficiency Assumption to a Principal Stress–Based Formulation for the Simulation of Anisotropic Bone Adaptation to Mechanical Loading", In *Proc. of the 1995 Bioengineering Conference*, R.M. Hochmuth *et al.* (Eds.), BED, Vol. **29**, ASME, New York, NY, pp. 447–478.

36 Katz, J.L. (1971), "Hard Tissue as a Composite Material I. Bounds on the Elastic Behavior", *J. Biomech.*, **4**, pp. 455–473.

37 Katz, J.L. (1981), "Composite Material Models for Cortical Bone", In *Mechanical Properties of Bone*, S.C. Cowin (Ed.), AMD, Vol. **45**, ASME, New York, NY, pp. 171–184.

38 Katz, J.L. and Meunier, A. (1990), "A Generalized Method for Characterizing Elastic Anisotropy in Solid Living Tissues", *J. Mat. Sci. Mater. in Med.*, **1**, pp. 1–8.

39 Krach, W., Reiter, T.J., Rammerstorfer, F.G. and Zenz, P. (1995), "Computerunterstützte Vorhersage des Knochenumbaus am Beispiel von Knieendoprothesen", In *Proc. d. 19. Jahrestagung der österr. Biomedizinischen Technik*, Biomedizinische Technik Band 40, Ergänzungsband 2, Schiele & Schön, Berlin, GFR, pp. 78–80.

40 Kummer, B.K.F. (1972), "Biomechanics of Bone: Mechanical Properties, Functional Structure, Functional Adaptation", In *Biomechanics: Its Foundation and Objectives*, Y.C. Fung (Ed.), Prentice–Hall, Englewood Cliffs, NJ, pp. 237–271.

41 Lees, S. and Davidson, C.L. (1977), "The Role of Collagen in the Elastic Properties of Calcified Tissues", *J. Biomech.*, **10**, pp. 473–486.

42 Lipson, S.F. and Katz, J.L. (1984), "The Relationship Between Elastic Properties and Microstructure of Bovine Cortical Bone", *J. Biomech.*, **17**, pp. 231–240.

43 Martin, R.B. and Burr, D.B. (1989), "*Structure, Function and Adaptation of Compact Bone*", Raven Press, New York, NY.

45 Martin, R.B. (1984), "Porosity and Specific Surface of Bone", In *CRC Critical Reviews in Biomedical Engng.*, **10**, CRC Press, Boca Raton FL, pp. 179–222.

46 McElhaney, J.H., Alem, N. and Roberts, V. (1970), "A Porous Block Model for Cancellous Bone", *ASME Publication 70-WA/BHF-2*, pp. 1–9.

47 Misra, J.C. and Samanta, S. (1987), "Effect of Material Damping on Bone Remodeling", *J. Biomech.*, **20**(3), pp. 241–249.

48 Müller, R. (1994), "3D Assessment and Analysis of Trabecular Bone Architecture", PhD. Thesis, ETH Zürich, Zurich.

49 Pauwels, F. (1965), "*Gesammelte Abhandlungen zur funktionellen Anatomie des Bewegungsapparates*", Springer–Verlag, Berlin.

50 Pedersen, P. (1989), "On Optimal Orientation of Orthotropic Materials", *Struct. Opt.*, **1**, pp. 101–106.

51 Pettermann, H. (1993), "Entwicklung eines Simulationsalgorithmus der natürlichen Anpassung des orthotropen Knochenmaterials", Diploma Thesis, Vienna University of Technology, Vienna.

52 Pettermann, H.E., Reiter, T.J. and Rammerstorfer, F.G. (1995), "Ein Simulationsalgorithmus der natürlichen Anpassung des orthotropen Knochenmaterials", In *Proc. d. 19. Jahrestagung der österr. Biomedizinischen Technik*, Biomedizinische Technik Band 40, Ergänzungsband 2, Schiele & Schön, Berlin, GFR, pp. 127–129.

53 Piekarski, K. (1973), "Analysis of Bone as a Composite Material", *Int. J. Engng. Sci.*, **11**, pp. 557–565.

54 Prendergast, P.J. and Taylor, D. (1992), "Design of Intramedullary Prostheses to Prevent Bone Loss: Predictions Based on Damage–Stimulated Remodelling", *J. Biomed. Engng.*, **14**, pp. 499–506.

55 Pugh, J.W., Rose, R.M. and Radin, E.L. (1973), "Elastic and Viscoelastic Properties of Trabecular Bone: Dependence on Structure", *J. Biomech.*, **6**, pp. 475–485.

56 Reilly, D.T., Burstein, A.H. and Frankel, V.H. (1974), "The Elastic Modulus for Bone", *J. Biomech.*, **7**, pp. 271–275.

57 Reiter, T.J., Rammerstorfer, F.G. and Böhm, H.J. (1990), "A Numerical Algorithm for the Simulation of Bone Remodeling", In *Advances in Bioengineering*, S.A. Goldstein (Ed.), BED, **17**, ASME, New York, NY, pp. 181–184.

58 Reiter, T.J. and Rammerstorfer, F.G. (1993), "Simulation of Natural Adaptation of Bone Material and Appli-cation in Optimum Composite Design", *Optimal Design with Advanced Materials*, P. Pedersen (Ed.), Elsevier, Amsterdam, pp. 25–36.

59 Reiter, T.J., Rammerstorfer, F.G. and Böhm, H.J. (1993a), "Computation of Biomechanical Effects in Bone Caused by Implants", In *Computer Methods in Mechanics*, Vol. II, W. Gilewski and L. Chodor (Eds), Kielce University of Technology, Kielce, pp. 799–806.

60 Reiter, T.J., Rammerstorfer, F.G. and Böhm, H.J. (1993b), "Structural Design Improvement by Functional Adaptation", In *Proc. of Structural Optimization 93*, J. Herskovits (Ed.), Rio de Janeiro, pp. 361–368.

61 Reiter, T.J., Böhm, H.J., Krach, W., Pleschberger, M. and Rammerstorfer, F.G. (1994a), "Some Applications of the Finite Element Method in Biomechanical Stress Analysis", *Int. J. Comput. Appl. Technol.*, **7**, pp. 233–241.

62 Reiter, T.J., Pettermann, H.E. and Rammerstorfer, F.G. (1994b), "Simulation of Bone Remodeling with Respect to Bone Anisotroy", In *Proc. of the 8th International Conference on Biomedical Engineering*, J.C.H. Goh and A. Nather (Eds), Singapore, pp. 201–203.

63 Reiter, T.J. (1995), "Knochen - eine selbstoptimierende Struktur?", In *Evolution und Optimierung: Strategien in Natur und Technik*, U. Kull and E. Ramm and R. Reiner (Eds), S. Hierzel Wissenschaftliche Verlagsgesellschaft Stuttgart, GFR, pp. 121–135.

64 Reiter, T.J. (1996), "Functional Adaptation of Bone and Application in Optimal Structural Design", VDI–Berichte, Reihe 17, Nr. 145, VDI-Verlag, Düsseldorf, GFR.

65 Rho, J.Y., Ashman, R.B. and Turner, Ch.H. (1993), "Young's Modulus of Trabecular and Cortical Bone Material: Ultrasonic and Microtensile Measurements", *J. Biomech.*, **26**, pp. 111–119.

66 Rice, J.C., Cowin, S.C. and Bowman, J.A. (1988), "On the Dependence of the Elasticity and Strength of Cancellous Bone on Apparent Density", *J. Biomech.*, **21**, pp. 155–168.

67 Van Rietbergen, B., Weinans, H., Huiskes, R. and Odgaard, A. (1995), "A New Method to Determine Trabecular Bone Elastic Properties and Loading Using Micromechanical Finite Element Models", *J. Biomech.*, **28**, pp. 69–81.

68 Starke, G.R., Mercer, C.D., Spirakis, A., Martin, J.B. and Learmonth, I.D. (1992), "Some Aspects of Adaptive Bone Growth as a Result of Total Hip Joint Replacement", In *Proc. 1992 ABAQUS Users' Conference*, HKS Inc., Providence, RI, pp. 483–496.

69 Suquet, P.M. (1990), "Une méthode simplifiée pour le calcul des proprietés élastiques de matériaux hétérogènes à structure périodique", *C. R. Acad. Sci. Paris, série II*, **311**, pp. 769–774.

70 Townsend, P.R., Raux, P., Rose, R.M., Miegel, R.E. and Radin E.L. (1975), "The Distribution and Anisotropy of the Stiffnesses of Cancellous Bone in the Human Patella", *J. Biomech.*, **8**, pp. 363–367.

71 Turner, C.H., Cowin, S.C., Rho, J.Y., Ashman, R.B. and Rice, J.C. (1990), "The Fabric Dependence of the Orthotropic Elastic Constants of Cancellous Bone", *J. Biomech.*, **23**, pp. 549–561.

72 Van Buskirk, W.C. and Ashman, R.B. (1981), "The Elastic Moduli of Bone", In *The Mechanical Properties of Bone*, S.C. Cowin (Ed.), AMD, **45**, ASME, New York, pp. 131–143.

73 Viceconti, M. and Seireg, A. (1990), "A Generalized Procedure for Predicting Bone Mass Regulation by Mechanical Strain", *Calcif. Tiss. Int.*, **47**, pp. 296–301.

74 Whalen, R.T., Carter, D.R. and Steele, C.R. (1988), "Influence of Physical Activity on the Regulation of Bone Density", *J. Biomech.*, **21**, pp. 825–837.

75 Williams, J.L. and Lewis, J.L. (1982), "Properties of an Anisotropic Model of Cancellous Bone from the Proximal Tibial Epiphysis", *J. Biomech. Engng.*, **104**, pp. 50–56.

76 Wolff, J. (1892), *Das Gesetz der Transformation der Knochen*, Hirschwald, Berlin.

77 Zysset, P.K. and Curnier, A. (1995), "An Alternative Model for Anisotropic Elasticity of Trabecular Bone", In *Proc. of the 1995 Bioengineering Conference*, R.M. Hochmuth *et al.* (Eds), BED, **29**, ASME, New York, NY, pp. 359–360.

APPENDIX

Poisson numbers in the unified model (for explanation see text)

Spongy Bone

Prismatic–Type Structure

$$\nu_{12} = \nu_{13} = \nu_T \tag{A1}$$

$$\nu_{23} = (\nu_x - \nu_T)\beta_3 + 3\nu_T - 2\nu_x \quad \text{with} \quad \nu_x = (1-\nu_T)\beta_2 + 3\nu_T - 2 \tag{A2}$$

Plated–Type Structure

$$\nu_{12} = \nu_T \tag{A3}$$

$$\nu_{13} = \nu_{23} = (\nu_x - \nu_T)\beta_3 + 3\nu_T - 2\nu_x \quad \text{with} \quad \nu_x = \nu_T(\beta_2 - 1) \tag{A4}$$

Cortical Bone

Prismatic–Type Structure

$$\nu_{12} = \nu_T + (\nu_{C12} - \nu_T)\hat{\rho} \tag{A5}$$

$$\nu_{13} = \nu_T + (\nu_{C13} - \nu_T)\hat{\rho} \tag{A6}$$

$$\nu_{23} = \nu_{t23} + (\nu_x - \nu_{t23})\hat{\rho} \quad \text{with} \quad \nu_{t23} \text{ from eq.(A2)} \tag{A7}$$

$$\text{and} \quad \nu_x = \frac{\nu_{C12} + \nu_{C23}}{2} + (\nu_{C23} - \frac{\nu_{C12} + \nu_{C23}}{2})(\beta_2 - 2) \tag{A8}$$

Plated–Type Structure

$$\nu_{12} = \nu_T + (\nu_{C12} - \nu_T)\hat{\rho} \tag{A9}$$

$$\nu_{13} = \nu_{t13} + (\nu_{xr} - \nu_{t13})\hat{\rho} \quad \text{with} \quad \nu_{t13} \text{ from eq.(A4)} \tag{A10}$$

$$\text{and} \quad \nu_{xr} = \nu_T + (\nu_{C13} - \nu_{C12})(\beta_2 - 1) \tag{A11}$$

$$\nu_{23} = \nu_{t23} + (\nu_x - \nu_{t23})\hat{\rho} \quad \text{with} \quad \nu_{t23} \text{ from eq.(A4)} \tag{A12}$$

$$\text{and} \quad \nu_x = \frac{\nu_{C12} + \nu_{C23}}{2} + (\nu_{C12} - \frac{\nu_{C12} + \nu_{C23}}{2})(2 - \beta_2) \tag{A13}$$

Please address your comments or questions on this paper to:
International Center for Numerical Methods in Engineering
Edificio C-1, Campus Norte UPC
Gran Capitán s/n
08034 Barcelona, Spain
Phone: 34-3-4016035; Fax: 34-3-4016517